Statistical Simulation of a Multi-Phase Tool Machining a Multi-Phase Workpiece

Swetlana Herbrandt, Uwe Ligges, Manuel Ferreira, Michael Kansteiner, and Claus Weihs

Abstract The continuing development of the multi-phase material concrete leads to an increased demand for the optimization of diamond impregnated tools. Because of high initial investment costs for diamond tools, not only the reduction of processing time, but also the reduction of tool wear is in the focus of interest. While some parameters like cutting speed can be controlled, other important parameters like the number of cutting diamonds are beyond our influence. To manage this randomness, simulation models for diamond and segment grinding are developed. In this work we will present two models for a segment grinding simulation. The first model is an extension of the simulation model proposed by Raabe et al. (2011) for single diamond scratching on basalt. Beside the goodness-of-fit, the simulation time is an essential factor in the development and choice of simulation models. The difficulties encountered while extending this model are discussed and we provide a solution to accelerate the workpiece simulation. In order to achieve a further reduction of simulation time, a second model is introduced under the assumption of pyramidal shaped diamonds. The

Swetlana Herbrandt · Uwe Ligges · Claus Weihs
TU Dortmund, Department of Statistics,
✉ [herbrandt,ligges,weihs]@statistik.tu-dortmund.de
Manuel Ferreira
TU Dortmund, Institute of Materials Engineering,
✉ manuel.ferreira@tu-dortmund.de
Michael Kansteiner
TU Dortmund, Institute of Machining Technology,
✉ michael.kansteiner@tu-dortmund.de

simulation results are compared with single diamond experimental data and a feasibility study is performed for the segment setup.

1 Introduction

The machining of mineral subsoil is daily routine at building sites. In many cases the machined material is concrete and the preferred tool for trepanning is a diamond impregnated drill because of the diamond's cutting properties. Since these tools are in general not adapted to particular situations, under certain circumstances the tool wear can be much higher than expected and would therefore lead to an earlier need for replacement. Hence our main target is the understanding and optimization of the machining process with simultaneous reduction of tool wear. The difficulty of this task is in the complexity of the process in conjunction with the problem that many variables affecting the machining process can not be directly influenced and are even difficult to observe. The simulation should enable the control of these parameters and offer the possibility to conduct as many simulated experiments as necessary to find optimal settings for tool production and the machining process.

In the last twenty years many different models for the simulation of forces, material removal and temperature in grinding processes were presented (Brinksmeier et al, 2006). The model categories range from heuristic and empirical to physical models, while high performance computers allow for the computation of models with resolution degrees from macroscopic to microscopic. The considered areas of application are as various as the models due to the versatile usability of diamond impregnated tools, the diverse characteristics of machined materials, and the multiple kinds of machining processes. The state of the art method for simulations of engineering applications like grinding or sawing is the finite elements approach (Zienkiewicz and Taylor, 1977; Altintas et al, 2005). Originally, this method is used for the description of continuous transformation of machined material regarding e.g. its deformation or the change in temperature. Therefore, the finite elements method is particularly suitable for materials which allow plastic or elastic deformation, respectively effects which cause a continuous change on the material. In the case of rigid materials, like natural stone, the material removal is a discontinuous process resulting in brittle fracture and discontinuous chip formation (Denkena et al, 2004). Such situa-
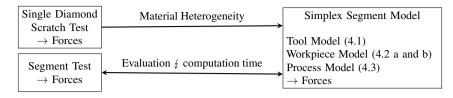
Single Diamond Scratch Test → Forces	Material Heterogeneity	Simplex Segment Model
		Tool Model (4.1) Workpiece Model (4.2 a and b) Process Model (4.3) → Forces
Segment Test → Forces	Evaluation ↯ computation time	

Fig. 1 Development of the Simplex Segment Model.

tions are often solved by the discrete elements approach or by a combination of both methods (Munjiza et al, 1995).

Raabe et al. (2011) considered a model for the force simulation of a single diamond grinding process with a geometrically undefined cutting edge scratching on basalt. Their approach is closely related to the discrete elements method since the removal mechanism is simulated by removing parts from a workpiece represented by a set of 3-dimensional simplexes. The resulting forces are calculated using a geometrical approach involving the angles of the interacting simplexes of diamond and workpiece. In the following papers the model was extended by including the material heterogeneity (Raabe et al, 2012) and compared with experimental data (Weihs et al, 2014). Continuing this work we introduce two models with further extensions concerning the material (from basalt to concrete) and the tool (from single diamond to a segment).

2 Outline

In this work we present two different models (Simplex Segment Model in Sect. 4 and Scratch Track Model in Sect. 5) for the machining of concrete with a single tool segment. The concrete is assumed to consist of two aggregates, basalt and cement, while the segment is a sintered composite of uniformly distributed diamonds in a metal matrix (see Sect. 3 for details).

In Sect. 4 we present a model (Simplex Segment Model, see Fig. 1 for model development) for segment grinding as an extension of the single diamond model of Raabe et al (2011, 2012) and Weihs et al (2014). Two models for the workpiece simulation are described in Sect. 4.2. The representation of the multi-phase tool (segment) is explained in Sect. 4.1, followed by a draft version of the process simulation (Sect. 4.3), where we discuss the computational challenge concerning the simulation time of this segment model.
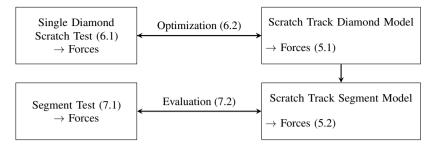
Single Diamond Scratch Test (6.1) → Forces	Optimization (6.2)	Scratch Track Diamond Model → Forces (5.1)
Segment Test (7.1) → Forces	Evaluation (7.2)	Scratch Track Segment Model → Forces (5.2)

Fig. 2 Development of the Scratch Track Model.

The computation time of this computationally expansive simulation is reduced by introducing an assumption about the geometry of the diamond's cutting profile. While the Simplex Segment Model is working with geometrically undefined cutting edges of the diamonds in the segment, the shape of the diamonds in the Scratch Track Model (see Fig. 2) in Sect. 5 is restricted to pyramids. This assumption allows the modeling of the scratch track which results when one or more diamonds scratch the surface of the workpiece. The development proceeds in two steps. In the first step we adjust all scratch track diamond model parameters by minimizing the deviation between observed forces from single diamond scratch tests and forces of the Scratch Track Diamond Model. For this we will first introduce the scratch track diamond model in Sect. 5.1, describe the experiments (Sect. 6.1) and then explain the optimization procedure and the results in Sect. 6.2. The second step is a feasibility study (Sect. 7.2) comparing the forces of the Scratch Track Segment Model (Sect. 5.2) with the forces of conducted experiments with segments (7.1).

The goal of this work is to predict the arising forces while drilling with the segment into concrete up to a predefined total depth with a constant cutting speed and a constant feed speed.

3 Grinding Process

The core drilling process is a widely used method in the construction industry. For this work diamond tipped drill core bits are used. A drill core bit consists of several rectangular segments attached to a circular body in equally spaced intervals. Each segment is a sintered composite of diamonds and metal powder. Due to a large number of influencing factors, measurement results gained from
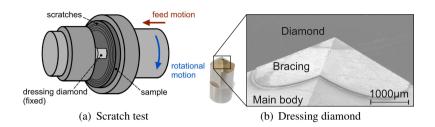
(a) Scratch test   (b) Dressing diamond

Fig. 3 Experimental setup for single diamond scratch test.

drilling tests provide only encapsulated information, because dependencies and interfaces cannot be distinguished clearly (Franca et al, 2015). Hence, the first logical step is to reduce the influencing factors by reducing the number of segments which are used for a drilling operation and therefore reducing the number of diamonds. Consequently, two different analysis approaches are studied. Tests with single diamonds, called scratch tests and tests with single segments comprising a number of diamonds on the surface.

Single Diamond Scratch Test To gain a better and more fundamental understanding of the complex grinding process, scratch tests with single diamonds are conducted (Fig. 3 (a)). The advantage of this procedure is the better process control due to the absence of diamond break outs, interactions between diamonds, and the influence of the metal matrix surrounding the diamonds in a segment. In the experimental setup a diamond with a pyramidal shape (Fig. 3 (b)) scratches on a circular path with radius r $[mm]$, a constant cutting speed v_c $\left[\frac{m}{min}\right]$ and a constant feed speed v_f $\left[\frac{mm}{min}\right]$ into the specimens until a total depth is reached. During the experiment the forces (tangential force f_x, radial force f_y, normal force f_z) are recorded.

Single Segment Test For single segment tests, the segments are manufactured in a powder metallurgical process route as a mixture of diamonds and metal powder. During the experiment the segment is attached to a tool holder (Fig. 4), so that the diamonds with workpiece contact scratch the workpiece on a circular path. As in the single diamond tests the cutting and feed speed are constant and the forces (tangential force f_x, radial force f_y, normal force f_z) are recorded.

Material Concrete is a composite material which consists of three main constituents: cement, water and aggregates. Due to chemical reactions between water and cement a hardening process occurs so that the cement acts like a
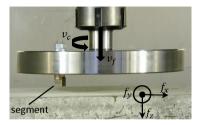
Fig. 4 Experimental setup for segment test.

binder which holds the aggregates together and builds a strong connection. Cement stone is a mixture of sand and water without aggregates like basalt.

4 Simplex Segment Model

The simplex model is a direct extension of the Raabe et al. (2011, 2012) model and consists of the three parts: tool, workpiece and process simulation.

4.1 Multi-Phase Tool

Diamond Assuming that all diamonds used for the segment production have the shape of truncated octahedra with different edge lengths, the two parameters $l_k = \frac{g}{2\sqrt{2}}$ and $c_k \in (0, l_k]$ (see Fig. 5 (a)) determine the geometrical form of a single diamond with size g. For simplicity in simulation, the truncated octahedron is subdivided into 3-dimensional simplexes as shown in Fig. 5 (c) by applying a Delaunay tessellation (Barber et al, 1996). Simplexes can be used to simulate the diamond wear by removing single simplexes from the diamond's simplex set. When considering the diamond wear, simplexes should be small and numerous. Since size and number of simplexes depend on the number of points used for the tessellation, such points have to be placed inside the truncated octahedron either at random positions or by creating a $3D$-lattice (Fig. 5 (b)). The lattice can be generated, e.g., by stringing together cubic diamond crystal structures as it was proposed by Raabe et al. (2012). The last step in the diamond simulation is a random rotation of all points.
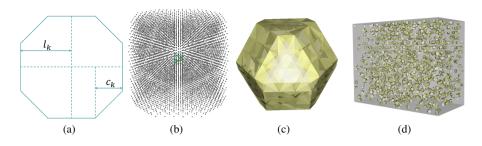
Fig. 5 (a) shape parameters, (b) cubic crystal structure lattice (c) simulated diamond (d) simulated segment with 5 vol.-% diamonds

Segment When moving from a single diamond towards a complete drill core bit, the segment is an intermediate step. As a sintered composite of diamonds and metal powder it introduces new parameters. Design parameters are shape and size of the segment, the size distribution of the diamonds, and their volume fraction ρ in the segment. Suppose, e.g., the diamond sizes g are uniformly distributed between 0.3 and 0.4 *mm* (equates to 40/50 mesh) and there are 5 vol.-% diamonds in the segment of size $a \times b \times c$ and volume $V_S = abc$. For the expected diamond size $E(g)$ the volume of this diamond is given by $V(E(g)) = 8\sqrt{2} \cdot 10^{-\frac{3}{2}} E(g)^3$. To get a diamond volume fraction of ρ there have to be

$$m = \frac{V_S}{V(E(g))} \rho$$

diamonds of size $E(g)$ in the segment. Therefore, we sample $\lfloor 2m \rfloor$ diamond sizes and determine the corresponding volumes $V(g_1), \ldots, V(g_{\lfloor 2m \rfloor})$. Sampling more sizes than probably needed provides us with the flexibility to reasonably approximate the volume fraction ρ. To achieve this, the first

$$n = \underset{1 \leq i \leq \lfloor 2m \rfloor}{\arg\min} \frac{\sum_{k=1}^{i} V(g_k)}{V_S} - \rho$$

sizes are taken for the diamonds placed in the segment. The positions $p_1, \ldots, p_n$ for these diamond sizes are sampled under the condition

$$\left\| p_k - p_j \right\| \geq \frac{g_{(k)} + g_{(j)}}{2} \quad \forall j < k$$

to guarantee that the diamonds do not overlap each other. For these positions the diamonds with sizes $g_1, \ldots, g_n$ are simulated as described above. A result is shown in Fig. 5 (d).
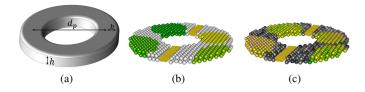
4.2 Multi-Phase Workpiece

In this section we will present two ideas for workpiece simulation which allow simulating concrete as a composite of different materials like basalt and cement, and reinforced concrete. The workpiece has the shape of a hollow cylinder with a height h and radii $r \pm b = \frac{d_p}{2} \pm b$, where the half width b of the cylinder must be greater than half the diamond size or half the segment width (Fig. 6 (a)).

   If we want to simulate reinforced concrete, we first need to simulate the reinforcing bar with diameter d_S. The position of this bar is given by an axis passing through two predefined or random points. Around this axis a point lattice is expanded. Then we create an equidistant cement grid with point distance δ_{coarse} on
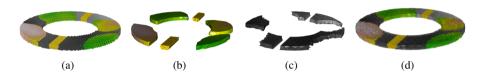
$$[-\lceil r+b \rceil, \lceil r+b \rceil] \times [-\lceil r+b \rceil, \lceil r+b \rceil] \times [0,h]$$

in steel direction to avoid irregular spacing between the bar and cement. To fill the cement grid with basalt grains, we repeat the next two steps until the desired basalt volume fraction is achieved. First we sample a random point from our coarse grid and a random grain diameter from the basalt diameter distribution $U(a_{\text{bas}}, b_{\text{bas}})$, where a_{bas} and b_{bas} are the lower and upper bound of the occurring basalt grain diameters. If there are no other grains (or steel) overlapping the sphere with the defined diameter around this random point, we define all points inside as basalt grain. The resulting workpiece grid is shown in Fig. 6 (b). Due to different material properties and inhomogeneity within the same material each point receives an intrinsic value according to its material. To achieve this, material specific exponential covariance functions are fitted from the estimated seasonality of the force time series of real basalt and cement experiments (Raabe et al, 2012). To use this information for each basalt grain grid and the remaining cement grid Gaussian random fields are sampled with the fitted covariance functions (see Fig. 6 (c)).

Approach a In the first steps all calculations are done on the coarse grid to save time. Since we want to degrade the workpiece into fragments by applying a Delaunay tessellation on the set of points from our grid, the distance between

Fig. 6 (a) Basic shape, (b) coarse grid with steel points (yellow), cement points (grey) and basalt points, (c) coarse grid after point elimination and (d) coarse grid with values (represented by different color shades) from sampled Gaussian random fields
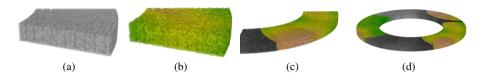

Fig. 7 (a) Finer grid with interpolated point values, (b) tessellation of basalt grains and reinforced bar, (c) tessellation of cement points and boundary points of the objects and (d) complete workpiece.

the points influences the size of the resulting tetrahedra. Due to the fact that the chip size (size of the removed material fragments) is very small we need a finer grid with point distance $\delta_{fine} < \delta_{coarse}$. The values for these grid points are interpolated by ordinary Kriging from the values of the coarse grid (Fig. 7 (a)). The Delaunay tessellation of the finer grid proceeds in two steps. We first apply it to the different workpiece objects (basalt grains, steel bar, Fig. 7 (b)). Then the remaining cement points and the boundary points of basalt and steel are degraded into simplexes (Fig. 7 (c)). It is obvious that especially in the second part of the workpiece tessellation the set of points is not convex. To handle this problem we remove all simplexes with maximal edge length greater than the 0.98–quantile of all maximal simplex edge lengths.

This procedure works much better than a tessellation of all points at once because it respects the boundaries of the single objects. Finally, each simplex receives the mean value of its four points' values which are of the same material as the simplex.

Approach b The most time consuming factor in the method of approach (a) is the Delaunay tessellation. To reduce this we provide a different approach. As described above we still need a finer grid but instead of expanding a finer grid over the whole workpiece shape, we just take one part of the hollow cylinder with the correct angle, being a fraction of π. By the Delaunay tessellation of

Fig. 8 (a) Workpiece blank, (b) first workpiece part with assigned simplex values, (c) four aligned workpiece parts and (d) complete workpiece consisting of sixteen aligned parts.

Table 1 Average values for 100 simulated concrete workpieces of the same size (standard deviation in parentheses).

	Approach a	Approach b
Points in finer grids	7504	11264
Point distance $[mm]$	0.33	0.251
Simplices	47578 (250)	47568 (0)
Mean simplex volume $[mm^3]$	$4.253 \cdot 10^{-3}$ $(9.973 \cdot 10^{-6})$	$2.623 \cdot 10^{-3}$ $(3.304 \cdot 10^{-6})$
Simulation time $[sec]$	37.147 (2.743)	10.716 (0.321)

this grid part we receive a degraded workpiece sector as shown in Fig. 8 (a) without point or simplex values. Since neither the points nor the simplexes of this sector have assigned values, we will call it a 'blank'. To create the workpiece, the next three steps have to be repeated until the hollow cylinder is complete (Fig. 8 (d)). A copy of the blank with jittered points is rotated to its position in the workpiece. Then we interpolate the values for the points of this part by ordinary Kriging from the values of the random fields of the coarse grid. Here we use the information about positions and sizes of the basalt grains for a material separated interpolation. Afterwards the values for the simplexes are calculated from the point values (Fig. 8 (b)). Because of using copies of the one blank, each part of the workpiece has the same Delaunay tessellation. Nevertheless, all simplexes have different volumes because we changed the basis of the tessellation by jittering the points in each part.

To compare the two workpiece simulations one hundred concrete workpieces with the sizes $d_p = 20\,mm$, $b = 2.5\,mm$ and a height of $h = 1\,mm$ were simulated for both procedures. Despite the fact that the numbers of simplexes are rather similar (see Table 1), the simulation time required for the second procedure is much shorter, as intended. Another advantage of the second workpiece simulation is that we have no variation in the number of simplexes because the blank tessellation does not depend on the material. That makes it easier to calculate the needed memory size.

4.3 Process Simulation

To simulate the machining process with workpieces as in Sect. 4.2 we first have to simulate a workpiece of desired size and material and a diamond or segment. After positioning the diamond or segment on the surface of the workpiece the process starts with the first movement of the tool. The length and depth of this movement depends on the cutting speed v_c, cutting depth per revolution $a_p = 10^{-3} \frac{v_f}{v_c} 2\pi r$ $[mm]$ and the number of iterations ν per revolution. For the simulation of N revolutions, we have to determine for each of the νN iterations whether the simulated tool has contact with the simulated workpiece. In this case the affecting forces are computed. When using a tool segment machining concrete, there are four possible interactions: basalt-diamond, basalt-metal matrix, cement-diamond and cement-metal matrix.

For the force calculation we can use a geometrical approach based on the edge orientation of the colliding simplexes and the division of the resulting force into radial and normal force described for the process with a single diamond in Raabe et al. (2012). In this approach each workpiece simplex hit by a diamond simplex is removed from the simulated workpiece. To extend this procedure to the grinding with a segment, we assume that material removal is only caused by the diamonds and not by the metal matrix. With the additional assumption that the force time signal is dominated by the forces arising in diamond-workpiece interaction, we only have to distinguish between the different workpiece materials. Nevertheless, in each iteration we have to determine each workpiece simplex with non-zero intersection volume with a simplex of at least one of the diamonds in the segment. The computation time of one iteration step depends on the number of simplexes in all diamonds and the number of simplexes in the workpiece. Since the whole number of simplexes decreases due to the wear and removal simulation, the evaluation of later iterations is faster. At the end of the process simulation many workpiece simplexes outside the scratch track will remain because they were not hit by any of the diamonds.

Unfortunately, it turned out that this model only appears to be appropriate for the simulation of short single diamond experiments but not for the much more complex simulation of segment experiments, which require the simulation of hundreds of revolutions with multiple diamonds. For this purpose, we developed another approach.

5 Scratch Track Model

In the new approach we reduce workpiece modeling to a minimum. Instead of modeling the complete workpiece and then remove parts of it, we only simulate the parts which are removed by the diamonds.

The shape of the diamond, introduced in Sect. 4.1, is simplified to a pyramid turned upside down as used in the single diamond experiments (Sect. 3). This simplification to a pyramidal form can be justified since the part of the octahedral diamond form that removes material in the segment experiments is very similar to a rotated pyramid. By this assumption, the resulting scratch track has the profile of a triangle with angle α determined by the cutting profile of the diamond.

Before we introduce the force model for the grinding process with a segment (5.2), we explain the model idea for the special case of a single diamond (5.1).

5.1 Scratch Track Diamond Model

In the one diamond case, a single diamond is scratching on a circular path along the workpiece surface (see Sect. 3). The maximal intrusion depth of the diamond is limited by the height of the diamond. For simplification we assume that this maximal depth is reached after N revolutions. Let denote v the number of modeled observations per revolution and $a_p = \frac{v_f}{v_c} 2\pi r$ the cutting depth per revolution. It is obvious that the resulting forces depend at least on the volume of removed material and characteristics of the machined material. Thus, in our model a realization of the modeled force is obtained by

$$F_i = \frac{g_{zv}}{r} \cdot z_i \cdot v_i + \frac{g_v}{r} \cdot v_i, \quad i = 1, \ldots, N\nu,$$

where r is the drilling radius, g_{zv} and g_v parameters, which have to be optimized, v_i the volume removed from the workpiece and z_i the material heterogeneity (Herbrandt et al, 2016). In the following we will describe the concept of the scratch track model and how the information about removed volume and material characteristics is linked to this scratch track.

To simulate v observations per revolution and N revolutions in total for one diamond, we place $vN + 1$ triangles evenly distributed along the diamond's scratch track (Fig. 9 (a)), whereby the first triangle has an area of zero. The sizes of these triangles depend on the intrusion depth of the diamond in the
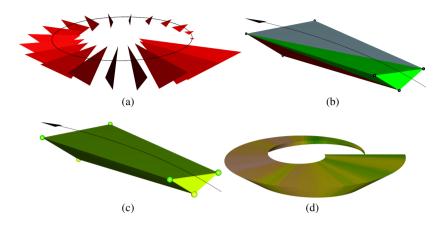
workpiece and the angle α of the pyramid representing the shape of the diamond. Since the cutting depth per revolution a_p is known, we can assume that the intrusion depth increases by $a = \frac{a_p}{v}$ for each simulated scratch track triangle D_j $(j = 1, \ldots, vN + 1)$ (see Fig. 9 (a) with the triangles $D_1, \ldots, D_{21}$ of the first revolution with $v = 20$). To consider the brittleness of the material, we allow a $Beta(0, a_p, p, q)$-distributed size variation $a^\star$ of the triangles, where $Beta(0, a_p, p, q)$ is the generalized beta distribution for the interval $[0, a_p]$ with the unknown parameters p and q. Thus, the height of the jth triangle D_j with the corner points (d_{j1}, d_{j2}, d_{j3}) is $h_j = a(j - 2) + a_j^\star$ $(j = 2, \ldots, Nv + 1$ and $h_1 = 0)$, where the i.i.d. variables $a_2^\star, \ldots, a_{vN+1}^\star$ have the same distribution as $a^\star$.

A simulated observation is represented by a scratch track part formed by the connection of two adjacent triangles (see Fig. 9 (b)). The connection is realized by three 3-dimensional simplexes and the removed volume v_i is calculated as the sum of the volumes of the three simplexes.

As in Sect. 4.2 the material heterogeneity is considered by sampling from Gaussian random fields. In contrast to Sect. 4.2, however, the number of values we have to sample from the Gaussian random fields is smaller, since only the $3(Nv + 1)$ points of the $Nv + 1$ triangles are taken into account. Additionally, we want to adjust the parameters $\mu, \sigma^2, \sigma_\xi^2, \psi$ of the Gaussian random field together with all the other parameters (p, q of the Beta distribution and g_{vz}, g_v) by minimizing the deviation between the observed and modeled forces (see Sect. 6.2). The material heterogeneity z_i of the ith modeled observation is calculated as the mean of the six sampled point values of each two adjoining triangles (d_{j1}, d_{j2}, d_{j3}) and $(d_{(j+1)1}, d_{(j+1)2}, d_{(j+1)3})$. In Fig. 9 (c) the six values are represented by the colors of the six points of the two triangles and the overall mean is represented by the color of the polyhedron (scratch track part) resulting by the connection of these two triangles. Fig. 9 (d) shows 100 of thus scratch track parts with heterogeneity values represented by colors in the first revolution.

5.2 Scratch Track Segment Model

In a segment we have several diamonds at random positions (see Sect. 3 and Sect. 4.1). In addition to the first assumption (diamond shape), we introduce a further assumption concerning the scratching with more than one diamond at
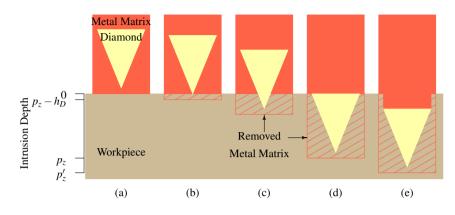
Fig. 9 (a) Scratch track triangles for the first revolution and (b) tessellation of one scratch track part into three simplexes (red, green and blue), (c) Scratch track part with sampled heterogeneity values for the six points represented by different color shades for the points and the mean value (color of track part) and (d) scratch track of the first revolution with $v = 100$ observations (scratch track parts) with assigned heterogeneity values.
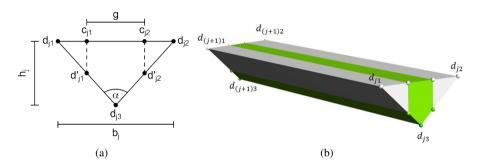
the same time. The second assumption states that the scratch tracks of different diamonds are independent of each other.

For our model one of the most important differences between grinding with a diamond and grinding with a segment (which corresponds to grinding with several diamonds) is the maximal intrusion depth. In the single diamond case this depth is determined by the diamond height, since the one diamond defines the complete tool. Therefore the intrusion depth ranges from 0 to the height of the diamond $h_D = \frac{g}{2\tan\frac{\alpha}{2}}$, where g is the diamond size and α the pyramid angle. In the segment experiment the diamonds are held by the metal matrix. Suppose that the position of the lowest diamond of size g and height h_D is $p = (p_x, p_y, p_z)^T$ (Fig. 10 (a)). Then the first contact of this diamond with the workpiece is at the intrusion depth of $p_z - h_D$ (Fig. 10 (b)). The Figs. 10 (b)–(d) show the intrusion period of this diamond. The diamond of height h_D is completely in the workpiece at the cutting depth of p_z (Fig. 10 (d)). When this maximal intrusion depth of the diamond is reached, the diamond is still held by the metal matrix and the grinding process proceeds (Fig. 10 (e)). We assume that the diamond breaks out at an unknown cutting depth p'_z.

The scratch track diamond model needs some adaptations for the segment application. The adaptations of the three model parts scratch track, volume and heterogeneity will be discussed in the same order as in Sect. 5.1.

Fig. 10 (a) First segment workpiece contact with a diamond (yellow) inside the metal matrix (red), (b) First diamond workpiece contact at a cutting depth of $p_z - h_D$, (c) Diamond in the intrusion period, (d) Diamond at the end of the intrusion period at a cutting depth of p_z, (e) Last position of the diamond before break out at p'_z.

Fig. 11 (a) jth scratch track triangle $D_j = (d_{j1}, d_{j2}, d_{j3})$ and diamond profile $(d'_{j1}, d'_{j2}, d_{j3})$ and (b) ith scratch track part

When modeling the scratch track we have to consider the case in Fig. 10 (e). When the length of the triangle's base $b_j = 2h_j \tan \frac{\alpha}{2}$ (h_j height of the jth triangle) representing the part of the diamond inside the workpiece exceeds the size of the diamond g, the intrusion period of the diamond has ended (as shown in Fig. 10 (d)). Since the diamond profile will not increase any more, we have to cut off the corners $\left(d_{j1}, d'_{j1}, c_{j1}\right)$ and $\left(d_{j2}, d'_{j2}, c_{j2}\right)$ (see Fig. 11 (a)) of the following scratch track triangles. The diamond's profile in the workpiece is determined by the triangles (d_{j1}, d_{j2}, d_{j3}) during the intrusion period and then by $\left(d'_{j1}, d'_{j2}, d_{j3}\right)$.

After the intrusion period the volume is reduced by the volumes v_{i1} (volume of the right grey polyhedron in Fig. 11 (b)) and v_{i2} (volume of the left grey polyhedron in Fig. 11 (b)) between the corresponding cut off corners. The resulting volume is the volume of the green polyhedron in Fig. 11 (b). Additionally, the volume v_i is reduced by the already removed volume v_{i-v} in the previous revolution for $i > v$ (same procedure as for the scratch track diamond model).

After that, the material heterogeneity z_i of the i-th modeled observation is calculated as the mean of the six sampled point values of each two adjoining diamonds' profile triangles (d_{j1}, d_{j2}, d_{j3}) and $(d_{(j+1)1}, d_{(j+1)2}, d_{(j+1)3})$ (as in the scratch track diamond model) or $(d'_{j1}, d'_{j2}, d'_{j3})$ and $(d'_{(j+1)1}, d'_{(j+1)2}, d'_{(j+1)3})$ after the intrusion period of the diamond (Fig. 11 (b)).

The resulting normal forces

$$F_i = \begin{cases} \frac{g_{zv}}{r} \cdot z_i \cdot v_i + \frac{g_v}{r} \cdot v_i, & p_z - h_D \leq a_{i+1} \leq p'_z \\ 0, & \text{otherwise} \end{cases}$$

are modeled so that for one diamond scratching at radius r and parameters g_{zv} and g_v normal forces increase as the removed volume v_i increases, while the variance is represented by the heterogeneity values z_i $(i = 1, \ldots, Nv)$. For K diamonds the total force in the ith iteration

$$F_{i,\text{total}} = \sum_{k=1}^{K} F_{i,k}$$

is determined as the sum of the K forces $F_{i,1}, \ldots, F_{i,K}$ in the ith iteration.

For the simulation of $Nv = 4500$ force observations with a segment including one diamond by using the presented scratch track segment model we need 9.83 (± 0.997) seconds. In almost the same time we can simulate the workpiece of the simplex segment model (approx. 10 seconds, see Table 1 in Sect. 4.2). For the simulation of 4500 observations with the simplex segment model we additionally need to simulate the process (Sect. 4.3) to calculate the forces. That means the scratch track segment model has finished the computation of 4500 observations even before the simplex segment model is ready to compute the first observation.

6 Single Diamond Grinding

In this section we will focus on the Scratch Track Diamond Model (Sect. 5.1). For the model parameter adjustment we first explain the details of the conducted single diamond experiments (Sect. 6.1) which provide the force data we use as reference in the adjustment procedure. Then the optimization of the model parameters and the results are presented (Sect. 6.2).

6.1 Design of Single Diamond Experiments

In the experimental setup a diamond scratches into the specimens until a total depth of $A = 0.08$ *mm*. During the experiment the forces (tangential force f_x, radial force f_y, normal force f_z) are recorded with a sampling rate of $v_f = 200000$ *Hz*. Depending on the total drilling depth and the speeds v_c and v_f, the total number of recorded observations per experiment and force can be calculated as $\frac{A \cdot 60}{v_f} v_f$ (here: between 101000 and 480000). The tests are conducted on a machining center (IXION TLF 1004) without a coolant or lubricant. For the analysis of the influence of the cutting speed $v_c \left[\frac{m}{min} \right]$ and the feed speed $v_f \left[\frac{mm}{min} \right]$ on the resulting process forces, a 4^2- full factorial design with the parameter setting $v_c \in \{40.5, 117, 193.5, 270\}$ and $v_f \in \{2, 4.5, 7, 9.5\}$ is chosen. By carrying out scratch tests on single phases of the composite material concrete the process is subdivided into subprocesses. Hence, tests on single phase basalt and cement stone are conducted to analyze the forces developing during the scratching. Five samples of each material are available and each of them can be scratched on 12 radii $r \in \{16, 17, \ldots, 27\}$ *mm*. The destructive testing does not allow real repetitions, so each speed combination (v_c, v_f) is repeated on adjacent radii of a sample. The 16 speed combinations of the full factorial design are distributed to six blocks of size five using the $D-$criterion.

Let denote $\mathscr{R}(v_c, v_f)$ the set of radii with the same speed combination (v_c, v_f) and $n_{\mathscr{R}}(v_c, v_f)$ the number of elements in this set. Since each speed combination is repeated on the adjacent radius, each set contains at least two elements.

6.2 Optimization of the Scratch Track Diamond Model

To find out whether the approach in Sect. 5 is suitable to describe forces arising during a single grain scratch test, the model parameters $\theta = (g_{zv}, \ g_v, \ \mu, \ \sigma^2, \ \sigma_\xi^2, \ \psi, \ p, \ q)$, where $\mu, \sigma^2, \sigma_\xi^2, \psi$ are the parameters of the Gaussian random field, are adjusted to the normal forces ($f_z = f$) from the conducted single grain experiments (see sec. 6.1) on basalt and cement (see Herbrandt et al, 2016, for more details). The adjustment is performed for each speed combination (v_c, v_f) by applying model based optimization techniques which are particularly suitable for the optimization of expensive black box functions (Jones et al, 1998). The target is the minimization of the objective function determining the deviation between observed and modeled forces. For this purpose the expected deviation

$$E\left(\left\|f\left(v_c, v_f, r\right) - \mathscr{F}\left(\theta, r\right)\right\|_D\right) = E\left(D\left(f\left(v_c, v_f, r\right), \mathscr{F}\left(\theta, r\right)\right)\right) \qquad (1)$$

of a measured force $f\left(v_c, v_f, r\right)$ from the model force $\mathscr{F}\left(\theta, r\right)$ (underlying force model process with realizations $F\left(\theta, r\right)$ as described in Sect. 5) is minimized. By estimating the expectation with the arithmetic average of M (here: $M = 25$) realizations F of the force model $\mathscr{F}$ and $n_{\mathscr{R}}\left(v_c, v_f\right)$ observed forces $f\left(v_c, v_f, r\right)$ with radii $r \in \mathscr{R}\left(v_c, v_f\right)$, the optimal parameter settings for one speed combination are obtained as

$$\theta^\star\left(v_c, v_f\right) = \underset{\theta \in \Theta}{\arg\min} \ \bar{D}\left(f\left(v_c, v_f\right), F\left(\theta\right)\right)$$

$$= \underset{\theta \in \Theta}{\arg\min} \ \frac{1}{3Mn_{\mathscr{R}}\left(v_c, v_f\right)} \sum_{r \in \mathscr{R}\left(v_c, v_f\right)} \sum_{m=1}^{M} \left[d_R\left(\widetilde{f}\left(v_c, v_f, r\right), \widetilde{F}\left(\theta, r\right)\right) \right. \qquad (2)$$

$$\left. + d_\beta\left(f^\star\left(v_c, v_f, r\right), F^\star\left(\theta, r\right)\right) + d_S\left(\widetilde{f}\left(v_c, v_f, r\right), \widetilde{F}\left(\theta, r\right)\right)\right],$$

where the terms are discussed in the following. The considered deviation measure $\bar{D}$ is the mean of measures for the comparison of the three characteristics slope, range, and spectrum. For the comparison the forces $f = f\left(v_c, v_f, r\right) = \left\{f_{t_i}\left(v_c, v_f, r\right) \mid 0 \le t_i \le T_f, \ i = 1, ..., L, \ L \text{ number of observations}, \ T_f \text{ observation time in seconds}\right\}$ and $F = F\left(\theta, r\right) = \left\{F_{t_i}\left(\theta, r\right) \mid 0 \le t_i \le T_F, \ i = 1, ..., Nv\right\}$ have to be aligned. Due to the different sampling rates and since the sampling rate of f is very high, we decide to exploit the characteristics of the time series, rather than applying very time consuming methods like the dynamic time

warping. Therefore, the forces f and F are aligned by the intercepts of the corresponding linear models

$$f = \beta_{f0} + \beta_{f1}t + \varepsilon_f \text{ and } F = \beta_{F0} + \beta_{F1}t + \varepsilon_F. \tag{3}$$

Therefore, the force with the smaller estimated intercept ($\widehat{\beta}_{f0}$ or $\widehat{\beta}_{F0}$) is shifted by redefining the starting time

$$f^\star = \begin{cases} f, & \widehat{\beta}_{f0} > \widehat{\beta}_{F0} \\ \left\{ f_{t_i} \mid 0 \le t_i - \frac{\widehat{\beta}_{F0} - \widehat{\beta}_{f0}}{\widehat{\beta}_{f1}} \le T_f - \frac{\widehat{\beta}_{F0} - \widehat{\beta}_{f0}}{\widehat{\beta}_{f1}} = T_{f^\star} \right\}, & \widehat{\beta}_{f0} \le \widehat{\beta}_{F0} \end{cases} \tag{4}$$

(F analogue). For the comparison of range and spectrum the forces are additionally detrended, so that

$$\widetilde{f} = \left\{ f_{t_i}^\star - \widehat{\beta}_{f^\star 0} - \widehat{\beta}_{f^\star 1} t_i \mid 0 \le t_i \le \min\left\{ T_{f^\star}, T_{F^\star} \right\} = T_{\widetilde{f}} \right\} \tag{5}$$

with $f^\star = \beta_{f^\star 0} + \beta_{f^\star 1}t + \varepsilon_{f^\star}$ (F analogue). Then the range difference is

$$d_R\left(\widetilde{f}, \widetilde{F}\right) = \left| \max_{0 \le t \le T_{\widetilde{f}}} \widetilde{f}_t - \min_{0 \le t \le T_{\widetilde{f}}} \widetilde{f}_t - \max_{0 \le t \le T_{\widetilde{F}}} \widetilde{F}_t + \min_{0 \le t \le T_{\widetilde{F}}} \widetilde{F}_t \right| \tag{6}$$

and the slope difference is

$$d_\beta\left(f^\star, F^\star\right) = \left| \widehat{\beta}_{f^\star 1} - \widehat{\beta}_{F^\star 1} \right|. \tag{7}$$

Since the modelled sampling rate

$$v_F = \frac{v v_c 10^3}{2\pi r 60} \quad \left[\frac{1}{s} \right] \tag{8}$$

is much smaller than the sampling rate $v_f \left[\frac{1}{s} \right]$ and we consider both time series on the same time interval, the number of considered observations $n_{\widetilde{F}}$ of F is also smaller than $n_{\widetilde{f}}$. Therefore, the spectral differences are only calculated at the Fourier frequencies

$$\varphi_j = \frac{j}{n} \text{ with } n = n_{\widetilde{F}} + \left| \min_{(a,b,c) \in \mathbb{N}^3} n_{\widetilde{F}} - 2^a 3^b 5^c \right| \text{ and } j = 1, \ldots, \left\lfloor \frac{n}{2} \right\rfloor \tag{9}$$

of the shorter time series $\widetilde{F}$. This approach allows the application of the fast Fourier transform (Bloomfield, 2004) algorithm, which by itself enables a fast computation of the periodogram

$$I_{\widetilde{F}}(\varphi_j) = \frac{1}{\nu_F n_{\widetilde{F}}} \left| \sum_{k=1}^{n_{\widetilde{F}}} \widetilde{F}_k \exp(-i2\pi\varphi_j k) \right|^2 \tag{10}$$

as an estimate of the spectrum of $\widetilde{F}$. By adjusting the angular frequencies $2\pi\varphi_j$ to the sampling rate of the measured signal $\widetilde{f}$, we obtain the periodogram

$$I_{\widetilde{f}}(\varphi_j) = \frac{1}{\nu_f n_{\widetilde{f}}} \left| \sum_{k=1}^{n_{\widetilde{f}}} \widetilde{f}_k \exp\left(-i2\pi\varphi_j \frac{\nu_F}{\nu_f} k\right) \right|^2 \tag{11}$$

of $\widetilde{f}$ at the same frequencies φ_j and can determine the spectral differences
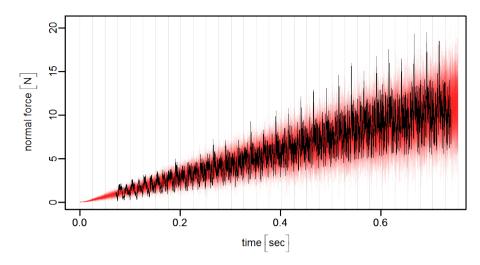
$$d_S\left(\widetilde{f},\widetilde{F}\right) = \sum_{j=1}^{\left\lfloor \frac{n}{2} \right\rfloor} \left| I_{\widetilde{f}}(\varphi_j) - I_{\widetilde{F}}(\varphi_j) \right|. \tag{12}$$

Since the scratch track diamond model is stochastic, the noisy Kriging model is chosen as surrogate in the model based optimization process for the CPU-intensive deviation function (Picheny et al, 2013). A new point for evaluation is proposed by maximizing the augmented expected improvement (Huang et al, 2006). We evaluated 800 parameter constellations θ for each speed combination (v_c, v_f). The first 80 points (initial design) for evaluation of the 800 in total were sampled from a random Latin hypercube.

The results achieved with this method show a good agreement between observed and modeled normal forces. Fig. 12 displays exemplarily the normal force from the conducted experiment for the speed combination $\big(v_c = 270 \frac{m}{min}, v_f = 7 \frac{mm}{min}\big)$ and 50 modeled force time series with optimized model parameters. As the figure implies, the modeled forces match the slope and variance of the observed force quite well.

Table 2 shows the optimization results for each of the 16 speed combinations (v_c, v_f). In the most cases the best parameters were found in the first 500 optimization steps. For the speed combinations with higher minimal deviation measures $\overline{D}_{\min}$ we observed discrepancies in the course of the corresponding force time series (repetitions with the same speed combination but on different radii or on different material samples). The described deviation measure results in small values if all 25 realizations of the scratch track diamond model fits in terms of slope, range and spectrum to all observed forces with the same speed combination. If the observed forces with the same speed combination are quite different, the optimal parameters found are a compromise which ensure the best fit of the modeled force for all these observations in terms of average.

Fig. 12 Normal force from conducted single grain experiment with the parameter settings $v_c = 270 \frac{m}{min}$, $v_f = 7 \frac{mm}{min}$, $r = 18$ mm (black) and 50 modeled forces (red).
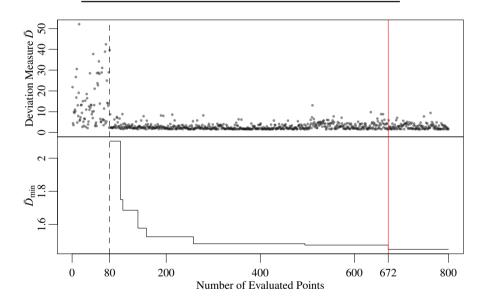
Fig. 13 is an example of an optimization course for the speed combination $v_c = 270 \frac{m}{min}$, $v_f = 7 \frac{mm}{min}$. The first 80 points are the realizations of the deviation measure for the model parameter combinations of the initial design (see upper figure in 13). By using the space filling random Latin hypercube design a good parameter combination with $\bar{D} \approx 2.1$ could already be found within these first 80 points (lower figure in 13). The iterative optimization improved this value in the following up to $\bar{D} \approx 1.45$ after the evaluation of 592 further points.

7 Single Segment Grinding

Since the resulting forces of the scratch track diamond model seems rather promising, we start the analysis of the scratch track segment model with a first feasibility study. In the first Subsect. (7.1) we summarize the technological details concerning the segment manufacturing, as well as the design of experiments for the conducted tests with the fabricated segments. The second Subsect. (7.2) will deal with the feasibility study and its results.

Table 2 Optimization results for the 16 speed combinations (v_c, v_f) with minimum value of $\overline{D}$ found and the according iteration $n_{\min}$ of the optimization procedure.

v_c	v_f	$\overline{D}_{\min}$	$n_{\min}$
40.5	2.0	3.245	328
40.5	4.5	3.037	621
40.5	7.0	5.643	682
40.5	9.5	4.317	299
117.0	2.0	1.492	800
117.0	4.5	3.811	490
117.0	7.0	7.075	427
117.0	9.5	4.413	434
193.5	2.0	1.657	731
193.5	4.5	3.729	171
193.5	7.0	1.749	452
193.5	9.5	6.950	423
270.0	2.0	2.089	122
270.0	4.5	4.750	755
270.0	7.0	1.450	672
270.0	9.5	7.607	261

Fig. 13 Optimization course for the speed combination $v_c = 270\ \frac{m}{min}$, $v_f = 7\ \frac{mm}{min}$. Upper Figure: Deviation measure $\overline{D}$ for the 800 parameter combinations of θ. Lower Figure: Minimal deviation measure from the first 80 evaluations (initial design) to all 800 evaluations. Red line marks the evaluation with the best found parameter combinations of θ.

7.1 Design of Single Segment Experiments

In the powder metallurgical process route a four component metal powder consisting of iron, cobalt, copper and tin (Diabase V21, Dr. Fritsch) is used, which is optimized for concrete machining. Within this process route synthetic diamonds (Syngrit SDB1055, Element Six) with varying grain sizes (20/30, 40/50 and 70/80 mesh) are added to the metal powder mixture at variable amounts of 2, 5 and 10 vol.-%. Subsequently the prepared powder-diamond material is homogenized in a tumbling mixer. Finally the raw material is filled in graphite moulds and sintered in a CSP100 hot-pressing facility (Dr. Fritsch) to shape geometries of 8×10 *mm* rectangles. The maximum pressure is $350 \frac{kg}{cm^2}$ and the sintering parameters are $840°$ C for three minutes. The single segment tests are carried out on a machining center (FZ 12 S, Chiron) under constant water supply. An additive within the water prevents corrosion of the machining center (Bechem Avantin 361, concentration 7 %). Before testing, segment dressing is carried out in order to expose the first diamond layer of the segment and thus, guarantee the contact between at least one diamond in the segment and the workpiece. The radius of the tool holder amounts to $r = 50$ *mm* (Fig. 4). Force measurements (tangential force f_x, radial force f_y, normal force f_z) are conducted using a force dynamometer (Kistler instruments, type 9255C) with a frequency of $v_f = 10000$ *Hz* until a total depth of $A = 3000$ *mm* is reached. For each diamond grain size and diamond concentration experiments with the parameter settings of a 3^2- full factorial design in circumferential speed $n = \frac{v_c 10^3}{2\pi r} \in \{117, 449, 781\}$ $\frac{1}{min}$ (rounds per minute) and feed velocity $v_f \in \{0.5, 1.25, 2\}$ $\frac{mm}{min}$ are performed (including repetitions).

7.2 Feasibility Study for the Scratch Track Segment Model

Since the model results for the scratch track diamond model are satisfactory, a feasibility study is established whether the scratch track segment model is able to reproduce a force time series from a conducted segment experiment (see Sect. 7.1). For this purpose the number of active diamonds and the number of broken out diamonds in the segment are fixed to be 15 and 1, respectively, for an experiment with circumferential speed $n = 449$ min^{-1}, $v_f = 2$ $\frac{mm}{min}$, grain size of 40/50 mesh and 2 vol.-% diamond concentration. Additionally, the $x-$ and

(a)   (b)
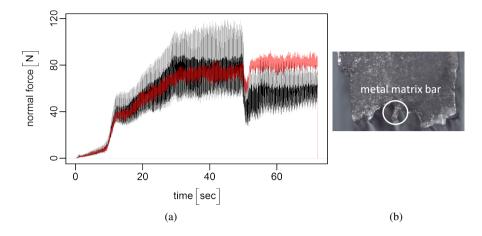
Fig. 14 (a) Normal forces of a segment experiment (black) and modeled forces with optimized parameters (red), (b) segment profile with marked metal matrix bar

y−coordinates of the diamonds' positions $p = (p_x, p_y, p_z)^T$ in the segment are measured.

According to the speed parameters the total cutting depth amounts to approximately 2.4 *mm*. Since 14 out of 15 cutting diamonds are still in the segment when the experiment is over, we have to set the end of the diamond-workpiece-interaction p'_z of these 14 diamonds to a value greater than 2.4 *mm*. For the broken out diamond the end of interaction is determined from the structural change in the force time series at approx. 1.67 *mm*. The remaining unknown parameters are the start of interaction of the 14 diamonds (one diamond's interaction starts at 0 *mm*), the grain sizes which are limited to the interval $[0.297, 0.4]$ *mm* corresponding to 40/50 mesh, and the diamonds' profile angles. The adjustment of all these parameters with the model based optimization (as described above) leads to the result presented in Fig. 14 (a). The average course is already well matched up to the point that one diamond breaks out after approx. 50 seconds. There are at least two explanations for this mismatch. One is that the optimized parameter settings are not correct for the broken out diamond. If the chosen grain size is too small or the diamond-workpiece-interaction starts too late, the resulting force of this diamond is too small at the break out point and thus would lead to a too small decrease in the force time series. Another explanation can be referred to a phenomenon that can be observed in segment experiments but not when using a drill core bit, where the material removal and the segment wear are more regular since more segments lead to more cutting

diamonds. If a diamond in a single segment is cutting along its circular path at a constant radius and there are no other diamonds at directly adjacent radii, the material to the left and to the right of this diamond is not removed. The result is that the metal matrix of the segment is removed at both sides of the diamond's position and the remaining metal matrix, which is holding the diamond, forms a bar (see Fig. 14 (b)). It is conceivable that the friction between this metal matrix bar and the workpiece results in higher forces. At the break out point the diamond and the metal matrix bar break out which would explain the much smaller forces after the break out. The magnitude of the normal force after the break out of the diamond depends on the size of the diamonds newly active afterwards.

8 Conclusion and Future Work

We have presented two different ways for the simulation of a grinding process. The first approach (in Sect. 4) is based on the tessellation of the workpiece into simplexes and turns out to require too much computation time. A reduction of the workpiece simulation time can be achieved using a slightly different approach (the 'blank'-approach) regarding the tessellation procedure. However, the computation of the process part cannot be accelerated without a substantial loss of accuracy. Therefore, the approach in Sect. 4 is certainly appropriate for the simulation of short single diamond experiments but not for the simulation of segment experiments, which require the simulation of hundreds of revolutions with multiple diamonds.

For this reason the approach in Sect. 5.1 was developed by introducing some assumptions about the scratch track produced by a pyramidal shaped diamond. The model parameters have been successfully adjusted to the data provided by the conducted single grain experiments (Sect. 6.1). Therefore, we performed a feasibility study (7.2) for the segment grinding simulation using the approach in Sect. 5.2 with one of the segment experiments as reference (Sect. 7.1). The average course of the normal force is already well matched by the modeled force. Thus, the presented model can be used as base for further developments. Improvements may be possible regarding the simulation time. Since all scratch track parts are subdivided into three simplexes in the same way, it is possible to derive a closed expression for the volume of each scratch track part and the volume for the scratch track reduction, respectively. This closed expression

will make the subdivision into simplexes redundant and thus leads to a faster calculation. We already derived such formulas for the scratch track diamond model (Herbrandt et al, 2016) and we want to extend these results for the presented scratch track diamond model.

  Beside the improvement of the actual model, future work will deal with the duration of the diamond-workpiece interaction. Based on the proposed simulations, future experiments will focus on a better understanding of diamond break outs depending on different compositions of the metal powder used for the segment manufacture.

References

Altintas Y, Brecher C, Weck M, Witt S (2005) Virtual machine tool. CIRP Annals-Manufacturing Technology 54(2):115–138, DOI 10.1016/ s0007-8506(07)60022-5

Barber CB, Dobkin DP, Huhdanpaa H (1996) The quickhull algorithm for convex hulls. ACM Transactions on Mathematical Software (TOMS) 22(4):469– 483, DOI 10.1145/235815.235821

Bloomfield P (2004) Fourier Analysis of Time Series: An Introduction. John Wiley & Sons, Hoboken, USA, DOI 10.1002/0471722235

Brinksmeier E, Aurich JC, Govekar C, Hoffmeister HW, Klocke F, Peters J, Rentsch R, Stephenson DJ, Uhlmann E, Weinert K, Wittmann M (2006) Advances in modeling and simulation of grinding processes. CIRP Annals-Manufacturing Technology 55(2):667–696, DOI 10.1016/j.cirp.2006.10.003

Denkena B, Becker JC, Gierse A (2004) Examination of basic separation mechanisms for machining concrete and stone. Production Engineering Research and Development 11(2):23–28

Franca LFP, Mostofi M, Richard T (2015) Interface laws for impregnated diamond tools for a given state of wear. International Journal of Rock Mechanics and Mining Sciences 73:184–193, DOI 10.1016/j.ijrmms.2014.09.010

Herbrandt S, Ligges U, Ferreira MP, Kansteiner M, Biermann D, Tillmann W, Weihs C (2016) Model based optimization of a statistical simulation model for single diamond grinding. Tech. rep., SFB 823 Discussion Paper 11/2016, TU Dortmund University

Huang D, Allen TT, Notz WI, Zeng N (2006) Global optimization of stochastic black-box systems via sequential kriging meta-models. Journal of Global Optimization 34(3):441–466, DOI 10.1007/s10898-005-2454-3

Jones DR, Schonlau M, Welch WJ (1998) Efficient global optimization of expensive black-box functions. Journal of Global Optimization 13(4):455–492, DOI 10.1023/A:1008306431147

Munjiza A, Owen D, Bicanic N (1995) A combined finite-discrete element method in transient dynamics of fracturing solids. Engineering Computations 12(2):145–174, DOI 10.1108/02644409510799532

Picheny V, Wagner T, Ginsbourger D (2013) A benchmark of kriging-based infill criteria for noisy optimization. Structural and Multidisciplinary Optimization 48(3):607–626, DOI 10.1007/s00158-013-0919-4

Raabe N, Rautert C, Ferreira M, Weihs C (2011) Geometrical process modeling and simulation of concrete machining based on delaunay tessellations. In: Ao SI, Douglas C, Grundfest WS, Burgstone J (eds) Proceedings of the World Congress on Engineering and Computer Science 2011 Vol II, WCECS '11, International Association of Engineers, Newswood Limited, Lecture Notes in Engineering and Computer Science, pp 991–996

Raabe N, Thieler AM, Weihs C, Fried R, Rautert C, Biermann D (2012) Modeling material heterogeneity by gaussian random fields for the simulation of inhomogeneous mineral subsoil machining. In: Dini P, Lorenz P (eds) SIMUL 2012: The Fourth International Conference on Advances in System Simulation, pp 97–102

Weihs C, Raabe N, Ferreira M, Rautert C (2014) Statistical process modelling for machining of inhomogeneous mineral subsoil. In: Gaul W, Geyer-Schulz A, Baba Y, Okada A (eds) German-Japanese Interchange of Data Analysis Results, Springer, Cham, CH, pp 253–263, DOI 10.1007/978-3-319-01264-3_22

Zienkiewicz OC, Taylor RL (1977) The Finite Element Method, vol 3. McGraw-hill, London